ABSTRACT

Title of Document: MODEL REDUCTION FOR NANOSCALE STICK-SLIP FRICTION USING PROPER ORTHOGONAL DECOMPOSITION.

Kristin Hadley O'Connor, Master of Science, 2006

Directed By: Associate Professor, Dr. Benjamin Shapiro, Department of Aerospace Engineering

Advances in computing hardware and algorithms have led to molecular dynamical models being able to model more realist cases. In this paper, we focus on a special case of molecular dynamics as a starting example. The molecular dynamical simulations that model slip-stick friction are often very large and complex, requiring a great deal of computational resources and time to run. In this paper, proper orthogonal decomposition (POD), a model reduction technique that has been successfully applied to a number of different application areas, is applied to the nanoscale slip-stick friction problem. The standard POD approach, and a modified version of the POD technique that is particularly aimed at the stick-slip problem, are presented.

MODEL REDUCTION FOR NANOSCALE STICK-SLIP FRICTION USING PROPER ORTHOGONAL DECOMPOSITION.

By

Kristin Hadley O'Connor.

Thesis submitted to the Faculty of the Graduate School of the
University of Maryland, College Park, in partial fulfillment
of the requirements for the degree of
Master of Science
2006

Advisory Committee:
Professor Benjamin Shapiro, Chair
Professor Stuart Antman
Professor John Osborn

Dedication

To my father, my first math teacher.

Acknowledgements

I would like to express my sincere appreciation to my advisor, Dr. Benjamin Shapiro, for his guidance and patience. Also, I would like to extend many thanks to my committee members, Dr. Stuart Antman and Dr. John Osborn.

Table of Contents

List of Tables

List of Figures

Chapter 1: Introduction

In classic physics, the experiment of sliding a block across a flat surface is often used to demonstrate the principles of friction. Leonardo da Vinci used a similar experiment to develop his theories on friction, theories which were later validated by Amontoms and Coulomb. (Gao, Luedtke, Gourdon, Ruths, Israelachvili and Landman, 3410-3411). As a result of the work of da Vinci, Amontoms, and Coulumb three laws of macroscopic friction were introduced: the frictional force is proportional to compression force, the frictional force is independent of the surface area between the two objects, and the friction force is independent of velocity at normal speeds. (Krim). "These classical laws of friction hold for a remarkably wide range of materials, but they are equally remarkable in terms of how difficult it is to derive them from fundamental atomic or molecular principles" (Krim). A great deal of research has focused on the basic physics at the small-scale level to better understand friction.(Singer) Advances in technology such as the atomic force microscope have allowed for friction at the microscopic level to be observed and have led to the discovery of the slip-stick phenomenon. (Shimizu, Eda, Yoritsune, and Ohmura, 118). "Studies of friction between atomically mica surfaces separated by an ultra thin layer of lubricant have revealed a striking phenomenon: in certain range of experimental parameters the fluid exhibits solid like properties, in particular, a critical yield stress leading to slip-stick similar to that in solid-on-solid dry friction processes" (Aranson, Tsimring, and Vinokur, 1). Molecular dynamic simulations have been very valuable in helping to understand this slip-stick behavior. These simulations often model hundreds of thousands of atoms and as a result any simulation can take a great deal of

time and computational resources to run. This paper presents two approaches for creating a reduced-order model capable of capturing the slip-stick behavior resulting from molecular friction at drastically reduced computational cost. This will allow such simulations to be included in device scale models for engineering analysis and design.

Proper Orthogonal Decomposition (POD), a technique that has been successfully applied to a number of different application areas (Rowley; Ly and Tran; Ravindran; Rowley, Colonius, and Murray), is applied here to the nanoscale slip-stick friction problem. This technique uses data from the full-scale model to construct a low-dimensional subspace. The POD approach is then coupled with a Galerkin Projection to produce a reduced-order model by projecting the dynamics of the original system onto the low-dimensional subspace.(Prajna, 2) In addition to the standard POD method, we developed a modified version that is particularly aimed at the stick-slip problem. This method attempts to correct one of the limitations of the standard POD technique that is an issue for us here: important dynamics may be under-represented in the dataset used in determining a low-dimensional subspace. For the nanoscale slip-stick problem, the dynamics of interest, the slip behavior, occurs very quickly and thus is only accounted for in a small percent of the collected data points. Our modified version of the standard POD involves dividing the data points into two separate sets based on whether the system is sticking or slipping at the data point and then using the standard POD method on the two subsets of data. The Galerkin Projection technique is then used with the combination of the results from the separate POD calculations to produce a reduced-order model.

This paper is organized as follows: Chapter 2 presents the simulation setup and describes the model used for this research. Chapter 3 presents the full model results. Chapter 4 outlines the Proper Orthogonal Decomposition technique along with the Galerkin Projection method that is combined with the POD to produce the reduced-order model. Chapter 5 then discusses how the standard POD approach was applied to the nanoscale slip-stick friction problem and presents results from this approach. The modified POD technique, along with its results, is presented in Chapter 6. Finally, Chapter 7 highlights some conclusions of this research and suggests areas where further research may be valuable. A nomenclature table is included in the Appendix for reference.

Chapter 2: Nanoscale Stick-Slip Friction Model

The model used for this paper is a very simple model, similar to the setup for a number of friction experiments (Aranson, Tsimring, and Vinokur, 1; Rozman, Urbakh, and Klafter, 683). In this simple, 2-dimensional model, a thin layer of lubricant atoms separates two crystal blocks with the top crystal attached to a spring that is pulled at a constant velocity. The crystal atoms are fixed in the crystal. For simplicity, the crystal blocks are only a single layer of equally-spaced atoms and all the atoms, lubricant and crystal, are assumed to be the same.

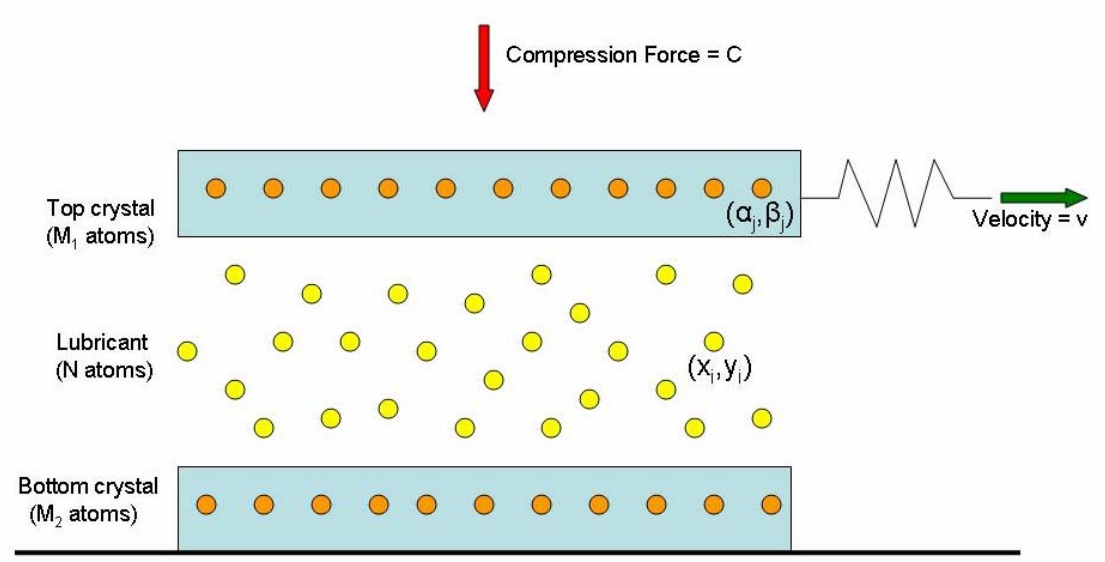

Figure 1: Model setup

The motion of each lubricant and crystal atom is restricted to the two-dimensional space (X,Y). The location of the i^{th} lubricant atom is represented by (x_i,y_i) and the location of the i^{th} crystal atom is represented by (α_i,β_i). Let the number of lubricant atoms be N and the number of crystal atoms by M. Furthermore, let M_1 be the number of fixed crystal atoms at the bottom of the model and M_2 be the number of crystal atoms making up the top, sliding crystal block. Then $M = M_1 + M_2$.

Also, assume that the top crystal block moves in the (X,Y) plane so that it stays horizontal; that is, there is no rotation. We let $\Delta\alpha$ and $\Delta\beta$ be the displacement of the top crystal block in the X and Y directions, respectively, and thus the motion of each crystal atom in the top block is $\alpha_i = \alpha_{i0} + \Delta\alpha$ and $\beta_i = \beta_{i0} + \Delta\beta$ where α_{i0} and β_{i0} is the location of atoms in the starting equilibrium state. By using m_{iLA} to represent the mass of the ith lubricant atom and m_{iCA} to represent the mass of the ith crystal atom, the kinetic energy of the system is

$$KE = \sum_{i=1}^{N} \frac{1}{2} m_{iLA} (\dot{x}_i^2 + \dot{y}_i^2) + \sum_{j=1}^{M_2} \frac{1}{2} m_{jCA} (\dot{\alpha}_j^2 + \dot{\beta}_j^2) \qquad (1)$$

Since $\dot{\alpha} = \dot{\Delta}\alpha$ and $\dot{\beta} = \dot{\Delta}\beta$ and the crystal atoms are fixed relative to each other,

$$KE = \sum_{i=1}^{N} \frac{1}{2} m_{iLA} (\dot{x}_i^2 + \dot{y}_i^2) + \sum_{j=1}^{M_2} \frac{1}{2} m_{jCA} (\dot{\Delta}\alpha^2 + \dot{\Delta}\beta^2)$$

$$= \sum_{i=1}^{N} \frac{1}{2} m_{iLA} (\dot{x}_i^2 + \dot{y}_i^2) + \frac{1}{2} M_2 m_{jCA} (\dot{\Delta}\alpha^2 + \dot{\Delta}\beta^2) \qquad (2)$$

For this model, the Lennard-Jones potential is used to representing the interaction of atoms. In general, atoms in close proximity to one another demonstrate a strong repulsive force on each other. As the atoms move further apart, the repulsive force becomes less and gradually turns into an attractive force. (Shapiro and Qian, 552) The Lennard-Jones (LJ) potential is an often used formula for calculating the potential energy between atoms or molecules (Robbins and Müser, 3). The potential is calculated by

$$u(r) = 4\varepsilon\left[\left(\frac{\sigma}{r}\right)^{12} - \left(\frac{\sigma}{r}\right)^{6}\right] \qquad (3)$$

where

$$r = \sqrt{(x_i - x_j)^2 + (y_i - y_j)^2} \qquad (4)$$

is the distance between atoms and ε and σ represent parameters describing the interaction between the atoms. The LJ potential, as shown in Figure 2 for $\varepsilon = 1$ and $\sigma = 1$, captures the repulsive force for atoms spaced less than r* and attractive force for atoms spaced greater than r* where r* is the equilibrium point of the LJ potential.

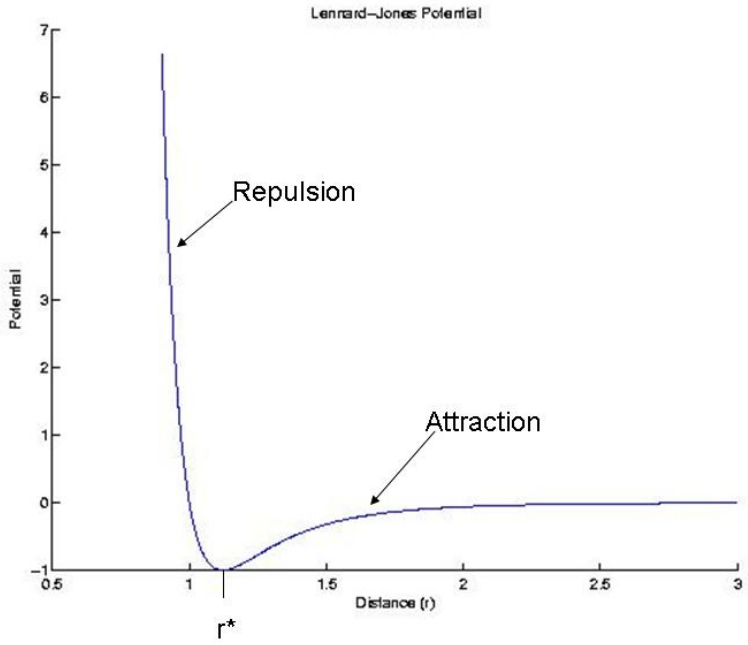

Figure 2: LJ potential for $\varepsilon = 1$ and $\sigma = 1$

As a result of using the Lenard-Jones potential, the potential energy of the system due to the interaction between atoms is

$$PE_A = \sum_{i=1}^{N}\sum_{\substack{j=1 \\ j\neq i}}^{N} 4\varepsilon\left[\sigma^{12}((x_i - x_j)^2 + (y_i - y_j)^2)^{-\frac{12}{2}} - \sigma^6((x_i - x_j)^2 + (y_i - y_j)^2)^{-\frac{6}{2}}\right]$$

$$+ \sum_{i=1}^{N}\sum_{j=1}^{M} 4\varepsilon\left[\sigma^{12}((x_i - \alpha_j)^2 + (y_i - \beta_j)^2)^{-\frac{12}{2}} - \sigma^6((x_i - \alpha_j)^2 + (y_i - \beta_j)^2)^{-\frac{6}{2}}\right]$$

$$+ \sum_{j=1}^{M_2}\sum_{\substack{i=1 \\ i\neq j}}^{M} 4\varepsilon\left[\sigma^{12}((\alpha_i - \alpha_j)^2 + (\beta_i - \beta_j)^2)^{-\frac{12}{2}} - \sigma^6((\alpha_i - \alpha_j)^2 + (\beta_i - \beta_j)^2)^{-\frac{6}{2}}\right] \quad (5)$$

For this simplified model, a spring, pulled at a constant velocity, is attached to the top crystal. The basic spring dynamics, governed by Hooke's Law, are used:

$$F = k\delta \qquad (6)$$

where k is the spring constant and δ is the displacement from the equilibrium position. In this experiment, our spring is being pulled at a constant velocity with the resulting force restricted to only the horizontal direction. The potential energy due to the external forces of the top crystal block is

$$PE_B = \sum_{j=1}^{M_2} C\beta_j + \sum_{j=1}^{M_2} \frac{1}{2}k(\alpha_j - \alpha_{j0} - vt)^2 \qquad (7)$$

where C is the compression force of the top crystal block, k is the spring constant, v is the velocity at which the top is being pulled at, and t is time. So, the total potential energy of the system is given by

$$PE = PE_A + PE_B \qquad (8)$$

The equations of motion for the system based on a standard Lagrange derivation (Wells) are:

$$\frac{d}{dt}\frac{\partial KE}{\partial \dot{x}_i}+\frac{\partial PE}{\partial x_i}=0 \qquad (9)$$

$$\frac{d}{dt}\frac{\partial KE}{\partial \dot{y}_i}+\frac{\partial PE}{\partial y_i}=0 \qquad (10)$$

$$\frac{d}{dt}\frac{\partial KE}{\partial \dot{\alpha}_j}+\frac{\partial PE}{\partial \alpha_j}=0 \qquad (11)$$

$$\frac{d}{dt}\frac{\partial KE}{\partial \dot{\beta}_j}+\frac{\partial PE}{\partial \beta_j}=0 \qquad (12)$$

where $i=1,\ldots,N$ and $j=1,\ldots,M_1$. Therefore, the equation of motion for the ith lubricant atom in the x-direction is

$$m_{iLA}\ddot{x}_i+\sum_{\substack{j=1\\ j\neq i}}^{N}4\varepsilon\left[-12\sigma^{12}(x_i-x_j)\left[(x_i-x_j)^2+(y_i-y_j)^2\right]^{-7}+6\sigma^{6}(x_i-x_j)\left[(x_i-x_j)^2+(y_i-y_j)^2\right]^{-4}\right]$$

$$+\sum_{j=1}^{M}4\varepsilon\left[-12\sigma^{12}(x_i-\alpha_j)\left[(x_i-\alpha_j)^2+(y_i-\beta_j)^2\right]^{-7}+6\sigma^{6}(x_i-\alpha_j)\left[(x_i-\alpha_j)^2+(y_i-\beta_j)^2\right]^{-4}\right]=0 \qquad (13)$$

Likewise the equation of motion for the ith lubricant atom in the y-direction is

$$m_{iLA}\ddot{y}_i+\sum_{\substack{j=1\\ j\neq i}}^{N}4\varepsilon\left[-12\sigma^{12}(y_i-y_j)\left[(x_i-x_j)^2+(y_i-y_j)^2\right]^{-7}+6\sigma^{6}(y_i-y_j)\left[(x_i-x_j)^2+(y_i-y_j)^2\right]^{-4}\right]$$

$$+\sum_{j=1}^{M}4\varepsilon\left[-12\sigma^{12}(y_i-\beta_j)\left[(x_i-\alpha_j)^2+(y_i-\beta_j)^2\right]^{-7}+6\sigma^{6}(y_i-\beta_j)\left[(x_i-\alpha_j)^2+(y_i-\beta_j)^2\right]^{-4}\right]=0 \qquad (14)$$

The equation of motion for the jth crystal atom in the top crystal block in the x-direction is

$$m_{iCA}\ddot{\alpha}_j + \sum_{i-1}^{N} 4\varepsilon\left[12\sigma^{12}(x_i-\alpha_j)\left[(x_i-\alpha_j)^2+(y_i-\beta_j)^2\right]^{-7} - 6\sigma^6(x_i-\alpha_j)\left[(x_i-\alpha_j)^2+(y_i-\beta_j)^2\right]^{-4}\right]$$

$$+\sum_{\substack{i=1\\ i\neq j}}^{M} 4\varepsilon\left[12\sigma^{12}(\alpha_i-\alpha_j)\left[(\alpha_i-\alpha_j)^2+(\beta_i-\beta_j)^2\right]^{-7} - 6\sigma^6(\alpha_i-\alpha_j)\left[(\alpha_i-\alpha_j)^2+(\beta_i-\beta_j)^2\right]^{-4}\right]$$

$$+k(\alpha_j-\alpha_{j0}-vt)=0 \qquad (15)$$

and in the y-direction is

$$m_{iCA}\ddot{\beta}_j + \sum_{i-1}^{N} 4\varepsilon\left[12\sigma^{12}(y_i-\beta_j)\left[(x_i-\alpha_j)^2+(y_i-\beta_j)^2\right]^{-7} - 6\sigma^6(y_i-\beta_j)\left[(x_i-\alpha_j)^2+(y_i-\beta_j)^2\right]^{-4}\right]$$

$$+\sum_{\substack{i=1\\ i\neq j}}^{M} 4\varepsilon\left[12\sigma^{12}(\beta_i-\beta_j)\left[(\alpha_i-\alpha_j)^2+(\beta_i-\beta_j)^2\right]^{-7} - 6\sigma^6(\beta_i-\beta_j)\left[(\alpha_i-\alpha_j)^2+(\beta_i-\beta_j)^2\right]^{-4}\right]+C=0 \qquad (16)$$

Summing all of the α_j equations together results in:

$$\sum_{j=1}^{M_2} m_{iCA}\ddot{\alpha}_j + \sum_{j=1}^{M_2}\sum_{i=1}^{N} 4\varepsilon\left[12\sigma^{12}(x_i-\alpha_j)\left[(x_i-\alpha_j)^2+(y_i-\beta_j)^2\right]^{-7} - 6\sigma^6(x_i-\alpha_j)\left[(x_i-\alpha_j)^2+(y_i-\beta_j)^2\right]^{-4}\right]$$

$$+\sum_{j=1}^{M_2}\sum_{\substack{i=1\\ i\neq j}}^{M} 4\varepsilon\left[12\sigma^{12}(\alpha_i-\alpha_j)\left[(\alpha_i-\alpha_j)^2+(\beta_i-\beta_j)^2\right]^{-7} - 6\sigma^6(\alpha_i-\alpha_j)\left[(\alpha_i-\alpha_j)^2+(\beta_i-\beta_j)^2\right]^{-4}\right]$$

$$+\sum_{j=1}^{M_2} k(\alpha_j-\alpha_{j0}-vt)=0 \qquad (17)$$

Now assume the masses of all crystal atoms are the same; $m_{CA}=m_{jCA}$ for all j. As defined earlier, $\alpha_j = \alpha_{j0} + \Delta\alpha$ for all j. Then,

$$\ddot{\alpha}_j = \ddot{\alpha}_{j0} + \ddot{\Delta}\alpha = \ddot{\Delta}\alpha$$

for all j. From this, it follows that

$$M_2 m_{CA}\ddot{\Delta}\alpha + \sum_{j=1}^{M_2}\sum_{i=1}^{N} 4\varepsilon\left[12\sigma^{12}(x_i-\alpha_j)\left[(x_i-\alpha_j)^2+(y_i-\beta_j)^2\right]^{-7} - 6\sigma^6(x_i-\alpha_j)\left[(x_i-\alpha_j)^2+(y_i-\beta_j)^2\right]^{-4}\right]$$

$$+\sum_{j=1}^{M_2}\sum_{\substack{i=1\\ i\neq j}}^{M} 4\varepsilon\left[12\sigma^{12}(\alpha_i-\alpha_j)\left[(\alpha_i-\alpha_j)^2+(\beta_i-\beta_j)^2\right]^{-7} - 6\sigma^6(\alpha_i-\alpha_j)\left[(\alpha_i-\alpha_j)^2+(\beta_i-\beta_j)^2\right]^{-4}\right]$$

$$+ M_2 k(\Delta\alpha - vt) = 0 \qquad (18)$$

Similarly, summing all of the β_j equations results in

$$M_2 m_{CA}\ddot{\Delta}\beta + \sum_{j=1}^{M_2}\sum_{i=1}^{N} 4\varepsilon\left[12\sigma^{12}(y_i-\beta_j)\left[(x_i-\alpha_j)^2+(y_i-\beta_j)^2\right]^{-7} - 6\sigma^6(y_i-\beta_j)\left[(x_i-\alpha_j)^2+(y_i-\beta_j)^2\right]^{-4}\right]$$

$$+\sum_{j=1}^{M_2}\sum_{\substack{i=1\\ i\neq j}}^{M} 4\varepsilon\left[12\sigma^{12}(\beta_i-\beta_j)\left[(\alpha_i-\alpha_j)^2+(\beta_i-\beta_j)^2\right]^{-7} - 6\sigma^6(\beta_i-\beta_j)\left[(\alpha_i-\alpha_j)^2+(\beta_i-\beta_j)^2\right]^{-4}\right]$$

$$+ M_2 C = 0 \qquad (19)$$

Lastly, we assume that the masses of all atoms, both crystal and lubricant, are the same; $m_{iLA} = m_{LA}$ for all i=1,…,N and the m_{CA}=m_{LA}=m_A.

<u>*Nondimensionalization of the Model*</u>

Nondimensionalization is a technique used to reduce the number of parameters in the system and to produce result independent of the units used. For the nondimensionalization of our model, we followed the approach used by Shapiro and Qian (553-554). In order to nondimensionalize the system, let $\tilde{x}_i = x_i / L_0$ for i=1,…,N where L_0 is some reference length. Let $\sigma = L_0$ be the spatial unit, then $\tilde{x}_i = x_i/\sigma$, $\tilde{y}_i = y_i/\sigma$, $\tilde{\alpha}_j = \alpha_j/\sigma$, $\tilde{\beta}_j = \beta_j/\sigma$, $\tilde{\Delta}\alpha = \Delta\alpha/\sigma$, and $\tilde{\Delta}\beta = \Delta\beta/\sigma$. The equation for the i[th] free lubricant atom in the x-direction becomes

$$\ddot{\tilde{x}}_i = \frac{\varepsilon}{m_A \sigma^2} \sum_{\substack{j=1 \\ j \neq i}}^{N} \left[48(\tilde{x}_i - \tilde{x}_j)\left[(\tilde{x}_i - \tilde{x}_j)^2 + (\tilde{y}_i - \tilde{y}_j)^2\right]^{-7} - 24(\tilde{x}_i - \tilde{x}_j)\left[(\tilde{x}_i - \tilde{x}_j)^2 + (\tilde{y}_i - \tilde{y}_j)^2\right)\right]^{-4} \right]$$

$$+ \frac{\varepsilon}{m_A \sigma^2} \sum_{j=1}^{M} \left[48(\tilde{x}_i - \tilde{\alpha}_j)\left[(\tilde{x}_i - \tilde{\alpha}_j)^2 + (\tilde{y}_i - \tilde{\beta}_j)^2\right]^{-7} - 24(\tilde{x}_i - \tilde{\alpha}_j)\left[(\tilde{x}_i - \tilde{\alpha}_j)^2 + (\tilde{y}_i - \tilde{\beta}_j)^2\right]^{-4} \right] \quad (20)$$

Let $\tilde{t} = t/\tau$ then $\tau(d\tilde{t}) = dt$ and $dt^2 = \tau^2(d\tilde{t}^2)$. It follows that

$\ddot{x} = \frac{d^2x}{dt^2} = \frac{d^2x}{\tau^2 d\tilde{t}^2} = \frac{1}{\tau^2} x''$. The equation for the i[th] free lubricant atom in the x-direction becomes

$$\tilde{x}_i'' = \frac{\tau^2 \varepsilon}{m_A \sigma^2} \sum_{\substack{j=1 \\ j \neq i}}^{N} \left[48(\tilde{x}_i - \tilde{x}_j)\left[(\tilde{x}_i - \tilde{x}_j)^2 + (\tilde{y}_i - \tilde{y}_j)^2\right)\right]^{-7} - 24(\tilde{x}_i - \tilde{x}_j)\left[(\tilde{x}_i - \tilde{x}_j)^2 + (\tilde{y}_i - \tilde{y}_j)^2\right]^{-4}) \right]$$

$$+ \frac{\tau^2 \varepsilon}{m_A \sigma^2} \sum_{j=1}^{M} \left[48(\tilde{x}_i - \tilde{\alpha}_j)\left[(\tilde{x}_i - \tilde{\alpha}_j)^2 + (\tilde{y}_i - \tilde{\beta}_j)^2\right]^{-7} - 24(\tilde{x}_i - \tilde{\alpha}_j)\left[(\tilde{x}_i - \tilde{\alpha}_j)^2 + (\tilde{y}_i - \tilde{\beta}_j)^2\right]^{-4}) \right] \quad (21)$$

Letting $\tau = \sigma\sqrt{m_A/\varepsilon}$ be the temporal unit results in

$$\tilde{x}_i'' = \sum_{\substack{j=1 \\ j \neq i}}^{N} \left[48(\tilde{x}_i - \tilde{x}_j)\left[(\tilde{x}_i - \tilde{x}_j)^2 + (\tilde{y}_i - \tilde{y}_j)^2\right]^{-7} - 24(\tilde{x}_i - \tilde{x}_j)\left[(\tilde{x}_i - \tilde{x}_j)^2 + (\tilde{y}_i - \tilde{y}_j)^2\right]^{-4} \right]$$

$$+ \sum_{j=1}^{M} \left[48(\tilde{x}_i - \tilde{\alpha}_j)\left[(\tilde{x}_i - \tilde{\alpha}_j)^2 + (\tilde{y}_i - \tilde{\beta}_j)^2\right]^{-7} - 24(\tilde{x}_i - \tilde{\alpha}_j)\left[(\tilde{x}_i - \tilde{\alpha}_j)^2 + (\tilde{y}_i - \tilde{\beta}_j)^2\right]^{-4} \right] \quad (22)$$

Repeating this procedure with the equation for the i[th] free lubricant atom in the y-direction yields

$$\tilde{y}_i'' = \sum_{\substack{j=1 \\ j \neq i}}^{N} \left[48(\tilde{y}_i - \tilde{y}_j)\left[(\tilde{x}_i - \tilde{x}_j)^2 + (\tilde{y}_i - \tilde{y}_j)^2\right]^{-7} - 24(\tilde{y}_i - \tilde{y}_j)\left[(\tilde{x}_i - \tilde{x}_j)^2 + (\tilde{y}_i - \tilde{y}_j)^2\right]^{-4} \right]$$

$$+ \sum_{j=1}^{M} \left[48(\tilde{y}_i - \tilde{\beta}_j)\left[(\tilde{x}_i - \tilde{\alpha}_j)^2 + (\tilde{y}_i - \tilde{\beta}_j)^2\right]^{-7} - 24(\tilde{y}_i - \tilde{\beta}_j)\left[(\tilde{x}_i - \tilde{\alpha}_j)^2 + (\tilde{y}_i - \tilde{\beta}_j)^2\right]^{-4}) \right] \quad (23)$$

The Δα and Δβ equations are nondimensionalized by using

$$\widetilde{K} = \frac{k\tau^2}{m_A}, \quad \widetilde{C} = \frac{C\tau^2}{m_A\sigma}, \quad \text{and } \widetilde{v} = \frac{v\tau}{\sigma}$$

The resulting nondimensionalized equations are

$$\Delta\widetilde{\alpha}'' = \frac{1}{M_2}\sum_{j=1}^{M_2}\sum_{i=1}^{N}\left[48(\widetilde{x}_i - \widetilde{\alpha}_j)\left[(\widetilde{x}_i - \widetilde{\alpha}_j)^2 + (\widetilde{y}_i - \widetilde{\beta}_j)^2\right]^{-7} - 24(\widetilde{x}_i - \widetilde{\alpha}_j)\left[(\widetilde{x}_i - \widetilde{\alpha}_j)^2 + (\widetilde{y}_i - \widetilde{\beta}_j)^2\right]^{-4}\right]$$

$$+\frac{1}{M_2}\sum_{j=1}^{M_2}\sum_{\substack{i=1\\ i\neq j}}^{M}\left[48(\widetilde{\alpha}_i - \widetilde{\alpha}_j)\left[(\widetilde{\alpha}_i - \widetilde{\alpha}_j)^2 + (\widetilde{\beta}_i - \widetilde{\beta}_j)^2\right]^{-7} - 24(\widetilde{\alpha}_i - \widetilde{\alpha}_j)\left[(\widetilde{\alpha}_i - \widetilde{\alpha}_j)^2 + (\widetilde{\beta}_i - \widetilde{\beta}_j)^2\right]^{-4}\right]$$

$$+\widetilde{K}(\Delta\widetilde{\alpha} - \widetilde{v}\widetilde{t}) \qquad (24)$$

$$\Delta\widetilde{\beta}'' = \frac{1}{M_2}\sum_{j=1}^{M_2}\sum_{i=1}^{N}\left[48(\widetilde{\beta}_j - \widetilde{y}_i)\left[(\widetilde{x}_i - \widetilde{\alpha}_j)^2 + (\widetilde{y}_i - \widetilde{\beta}_j)^2\right]^{-7} - 24(\widetilde{\beta}_j - \widetilde{y}_i)\left[(\widetilde{x}_i - \widetilde{\alpha}_j)^2 + (\widetilde{y}_i - \widetilde{\beta}_j)^2\right]^{-4}\right]$$

$$+\sum_{j=1}^{M_2}\sum_{\substack{i=1\\ i\neq j}}^{M}\left[48(\widetilde{\beta}_j - \widetilde{\beta}_i)\left[(\widetilde{\alpha}_i - \widetilde{\alpha}_j)^2 + (\widetilde{\beta}_i - \widetilde{\beta}_j)^2\right]^{-7} - 24(\widetilde{\beta}_j - \widetilde{\beta}_i)\left[(\widetilde{\alpha}_i - \widetilde{\alpha}_j)^2 + (\widetilde{\beta}_i - \widetilde{\beta}_j)^2\right]^{-4}\right] + \widetilde{C} \qquad (25)$$

Adding Dissipation to the Model

"In an experiment, heat flows away from the sliding interface into the surrounding solid. In simulations, the effects of the surrounding solid must be mimicked by coupling the particles to a heat bath" (Robbins and Müser, 3). A number of different techniques are often used in simulation to keep the temperature constant such as the Hoover-Nose' thermostat (Schall, Padgett, and Brenner, 283). Another method is the Langevin thermostat consists of a constant damping term and a randomly distributed force. (He and Robbins, 3). For this very simple model, just a constant damping term is used to remove energy from the system. This damping term is applied only to the lubricant atoms in both the x and y directions. The resulting equations of motion for the free lubricant atoms are:

$$\tilde{x}_i'' = \sum_{\substack{j=1 \\ j\neq i}}^{N}\left[48(\tilde{x}_i-\tilde{x}_j)\left[(\tilde{x}_i-\tilde{x}_j)^2+(\tilde{y}_i-\tilde{y}_j)^2\right]^{-7}-24(\tilde{x}_i-\tilde{x}_j)\left[(\tilde{x}_i-\tilde{x}_j)^2+(\tilde{y}_i-\tilde{y}_j)^2\right]^{-4}\right]$$

$$+\sum_{j=1}^{M}\left[48(\tilde{x}_i-\tilde{\alpha}_j)\left[(\tilde{x}_i-\tilde{\alpha}_j)^2+(\tilde{y}_i-\tilde{\beta}_j)^2\right]^{-7}-24(\tilde{x}_i-\tilde{\alpha}_j)\left[(\tilde{x}_i-\tilde{\alpha}_j)^2+(\tilde{y}_i-\tilde{\beta}_j)^2\right]^{-4}\right]-d\tilde{x}_i' \quad (26)$$

$$\tilde{y}_i'' = \sum_{\substack{j=1 \\ j\neq i}}^{N}\left[48(\tilde{y}_i-\tilde{y}_j)\left[(\tilde{x}_i-\tilde{x}_j)^2+(\tilde{y}_i-\tilde{y}_j)^2\right]^{-7}-24(\tilde{y}_i-\tilde{y}_j)\left[(\tilde{x}_i-\tilde{x}_j)^2+(\tilde{y}_i-\tilde{y}_j)^2\right]^{-4}\right]$$

$$+\sum_{j=1}^{M}\left[48(\tilde{y}_i-\tilde{\beta}_j)\left[(\tilde{x}_i-\tilde{\alpha}_j)^2+(\tilde{y}_i-\tilde{\beta}_j)^2\right]^{-7}-24(\tilde{y}_i-\tilde{\beta}_j)\left[(\tilde{x}_i-\tilde{\alpha}_j)^2+(\tilde{y}_i-\tilde{\beta}_j)^2\right]^{-4}\right]-d\tilde{y}_i' \quad (27)$$

where d is the damping coefficient.

Thus, the final non-dimensional equations describing the model are:

$$\tilde{x}_i'' = \sum_{\substack{j=1 \\ j\neq i}}^{N}\left[\left[48((\tilde{x}_i-\tilde{x}_j)^2+(\tilde{y}_i-\tilde{y}_j)^2)^{-13}-24((\tilde{x}_i-\tilde{x}_j)^2+(\tilde{y}_i-\tilde{y}_j)^2)^{-7}\right]\frac{(\tilde{x}_i-\tilde{x}_j)}{\sqrt{(\tilde{x}_i-\tilde{x}_j)^2+(\tilde{y}_i-\tilde{y}_j)^2}}\right]$$

$$+\sum_{j=1}^{M}\left[\left[48((\tilde{x}_i-\tilde{\alpha}_j)^2+(\tilde{y}_i-\tilde{\beta}_j)^2)^{-13}-24((\tilde{x}_i-\tilde{\alpha}_j)^2+(\tilde{y}_i-\tilde{\beta}_j)^2)^{-7}\right]\frac{(\tilde{x}_i-\tilde{\alpha}_j)}{\sqrt{((\tilde{x}_i-\tilde{\alpha}_j)^2+(\tilde{y}_i-\tilde{\beta}_j)^2)}}\right]-d\tilde{x}_i' \quad (28)$$

$$\tilde{y}_i'' = \sum_{\substack{j=1 \\ j\neq i}}^{N}\left[\left[48((\tilde{x}_i-\tilde{x}_j)^2+(\tilde{y}_i-\tilde{y}_j)^2)^{-13}-24((\tilde{x}_i-\tilde{x}_j)^2+(\tilde{y}_i-\tilde{y}_j)^2)^{-7}\right]\frac{(\tilde{y}_i-\tilde{y}_j)}{\sqrt{((\tilde{x}_i-\tilde{x}_j)^2+(\tilde{y}_i-\tilde{y}_j)^2)}}\right]$$

$$+\sum_{j=1}^{M}\left[\left[48((\tilde{x}_i-\tilde{\alpha}_j)^2+(\tilde{y}_i-\tilde{\beta}_j)^2)^{-13}-24((\tilde{x}_i-\tilde{\alpha}_j)^2+(\tilde{y}_i-\tilde{\beta}_j)^2)^{-7}\right]\frac{(\tilde{y}_i-\tilde{\beta}_j)}{\sqrt{((\tilde{x}_i-\tilde{\alpha}_j)^2+(\tilde{y}_i-\tilde{\beta}_j)^2)}}\right]-d\tilde{y}_i' \quad (29)$$

$$\Delta\tilde{\alpha}'' = \frac{1}{M_2}\sum_{j=1}^{M_2}\sum_{i=1}^{N}\left[\left[48((\tilde{x}_i-\tilde{\alpha}_j)^2+(\tilde{y}_i-\tilde{\beta}_j)^2)^{-13}-24((\tilde{x}_i-\tilde{\alpha}_j)^2+(\tilde{y}_i-\tilde{\beta}_j)^2)^{-7}\right]\frac{(\tilde{\alpha}_j-\tilde{x}_i)}{\sqrt{((\tilde{x}_i-\tilde{\alpha}_j)^2+(\tilde{y}_i-\tilde{\beta}_j)^2)}}\right]$$

$$+\frac{1}{M_2}\sum_{j=1}^{M_2}\sum_{\substack{i=1 \\ i\neq j}}^{M}\left[\left[48((\tilde{\alpha}_i-\tilde{\alpha}_j)^2+(\tilde{\beta}_i-\tilde{\beta}_j)^2)^{-13}-24((\tilde{\alpha}_i-\tilde{\alpha}_j)^2+(\tilde{\beta}_i-\tilde{\beta}_j)^2)^{-7}\right]\frac{(\tilde{\alpha}_j-\tilde{\alpha}_i)}{\sqrt{((\tilde{\alpha}_i-\tilde{\alpha}_j)^2+(\tilde{\beta}_i-\tilde{\beta}_j)^2)}}\right]$$

$$+\tilde{K}(\Delta\tilde{\alpha}-\tilde{v}\tilde{t}) \quad (30)$$

$$\Delta\tilde{\beta}'' = \frac{1}{M_2}\sum_{j=1}^{M_2}\sum_{i=1}^{N}\left[\left[48((\tilde{x}_i-\tilde{\alpha}_j)^2+(\tilde{y}_i-\tilde{\beta}_j)^2)^{-13}-24((\tilde{x}_i-\tilde{\alpha}_j)^2+(\tilde{y}_i-\tilde{\beta}_j)^2)^{-7}\right]\frac{(\tilde{\beta}_j-\tilde{y}_i)}{\sqrt{((\tilde{x}_i-\tilde{\alpha}_j)^2+(\tilde{y}_i-\tilde{\beta}_j)^2)}}\right]$$

$$+\sum_{j=1}^{M_2}\sum_{\substack{i=1\\ i\neq j}}^{M}\left[\left[48((\tilde{\alpha}_i-\tilde{\alpha}_j)^2+(\tilde{\beta}_i-\tilde{\beta}_j)^2)^{-13}-24((\tilde{\alpha}_i-\tilde{\alpha}_j)^2+(\tilde{\beta}_i-\tilde{\beta}_j)^2)^{-7}\right]\frac{(\tilde{\beta}_j-\tilde{\beta}_i)}{\sqrt{((\tilde{\alpha}_i-\tilde{\alpha}_j)^2+(\tilde{\beta}_i-\tilde{\beta}_j)^2)}}\right]+\tilde{C} \quad (31)$$

Applying Periodic Boundary Conditions

By applying periodic boundary conditions to our model, we are able to focus on the behavior of the lubricant atoms as a result of the top crystal motion and avoid special considerations needed for border atoms. In this way, the model behaves as if of infinite length (Harrison, White, Colton, and Brenner, 46). The periodic boundary conditions are accomplished by adding a replication of the crystal and lubricant atoms to the left and to the right of the atoms of interest as shown in figure 3.

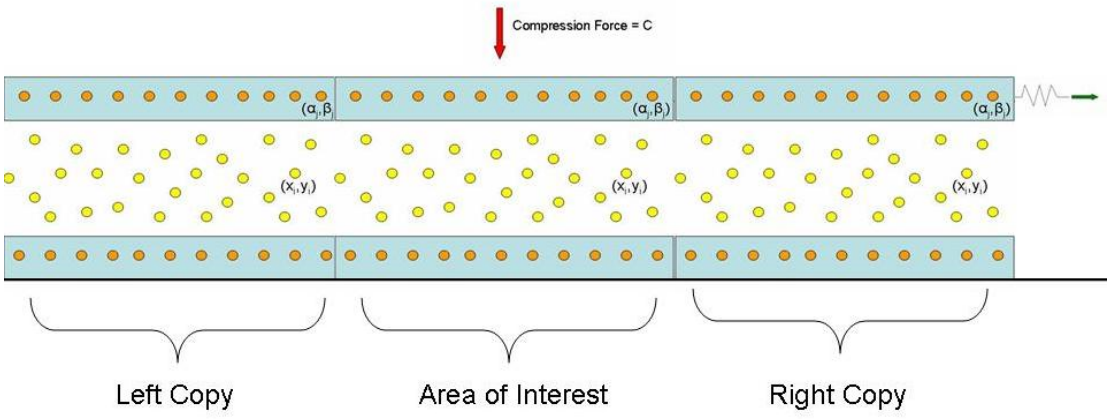

Figure 3: Periodic boundary conditions

Model Parameters

For this simulation, the damping coefficient was set to d=0.4 as was used by He and Robbins(3). With the damping coefficient set, we choose an arbitrary spring constant $\widetilde{K}$ = 20 and an arbitrary compression force $\widetilde{C}$ = 10. Once these values were set, a variety of different values were tried for velocity until a velocity was found that caused the top crystal to illustrate the stick-slip-stick behavior. The velocity value used in these simulations is $\widetilde{v}$ = 0.3.

Limitations of Model

As the goal of this paper is to demonstrate that Proper Orthogonal Decomposition is capable of producing a low-dimensional model for a large system where the top crystal demonstrates the stick-slip-stick behavior, our model is very simple. In simplifying the model, we assumed that all atoms were the same. In addition, this model consists of very few atoms compared to a realistic MD simulation. The crystal atoms were also only one layer of atoms thick. Lastly, we used a very crude damping to model heat dissipation. As a result, this model will not be accurate over an extended period of time.

Chapter 3: Full Model Results

Equilibrium

At the start of these experiments, all atoms are assumed to be at rest. A standard Newton's Method was implemented in Matlab to determine the equilibrium positions of the system. We used a variety of different starting configurations and found two different equilibrium positions. Figure 4 shows an equilibrium position where all of the atoms are arranged in vertical lines.

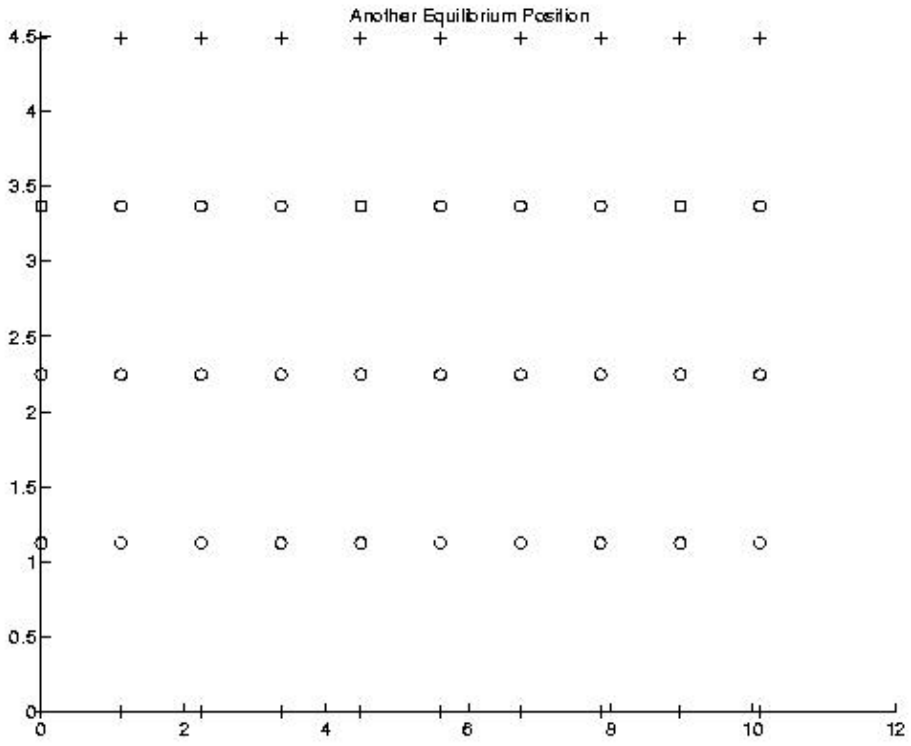

Figure 4: An Equilibrium configuration

Figure 5 shows the other equilibrium position where the atoms are arranged in a lattice formation.

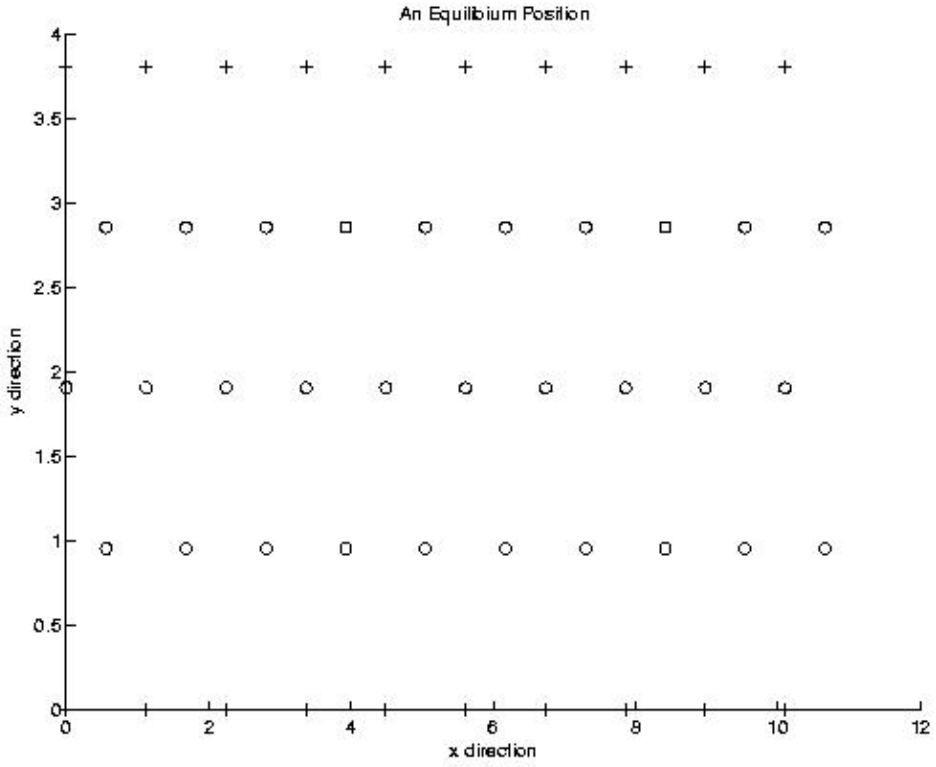

Figure 5: Another Equilibrium configuration

Stability

In order to determine the stability of a particular configuration, we focus on the curvature of the potential energy function in equation 5 describing the atomic interactions. The Hessian matrix, the square matrix of second partial derivative, describes the curvature of the potential energy function for a given arrangement of lubricant and crystal atoms. The eigenvalues of the Hessian matrix, *H*, can be used to determine the stability of a configuration. If the eigenvalues are all greater than zero,

the equilibrium position is stable and unstable if there exists an eigenvalue less than zero (Brakke, 3). Based on the calculations of eigenvalues for the Hessian matrices for each equilibrium configuration, the equilibrium position shown in Figure 4 is found to be unstable while the configuration shown in Figure 5 is found to be stable.

Simulation

Based on the equations of motion presented in Chapter 2, a simulation was set up by using Matlab. This model consisted of 4 variables ($\tilde{x}, \tilde{y}, \tilde{x}', \tilde{y}'$) for each lubricant atom and for 4 variables ($\tilde{\alpha}, \tilde{\beta}, \tilde{\alpha}', \tilde{\beta}'$) for each crystal atom. For this simple simulation, there were 30 free lubricant atoms and 20 crystal atoms, 10 of which were stationary. Thus, 160 variables would describe the position and velocity of each atom in the model. Representing the top crystal atom as a single unit reduced the system to 124 variables.

For this simple experiment, the time was set such that one full slip-stick cycle was captured ($\tilde{t} = 10$). Figure 6 shows the trajectories of free atoms for the full-scale model simulation.

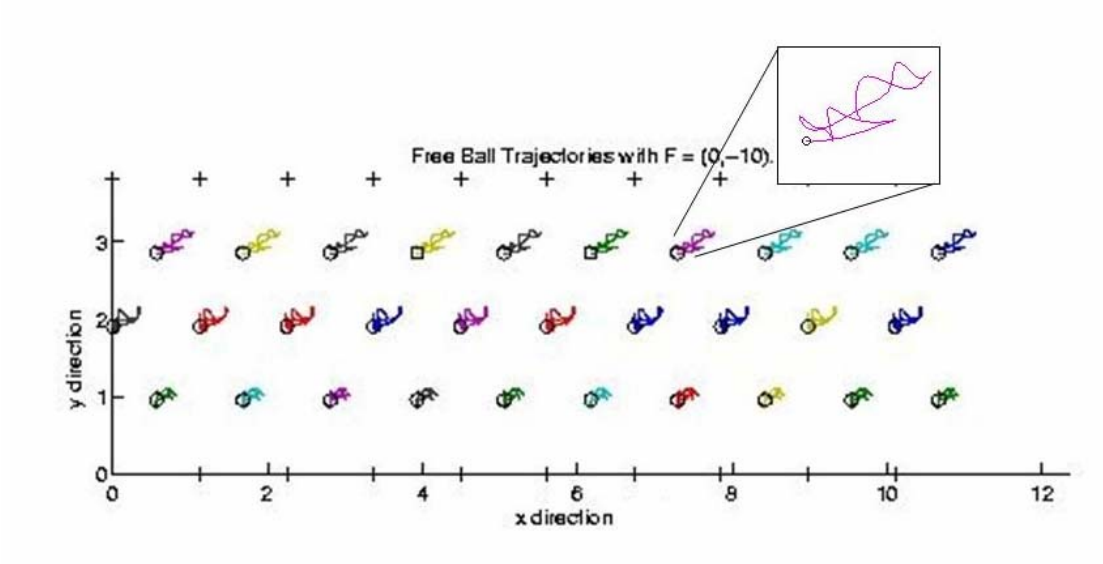

Figure 6: Atom trajectories for full-scale simulation

The stick-slip behavior can be seen by looking at the movement of the top crystal. Figure 7 is a plot of the x-position of the top crystal as a function of time.

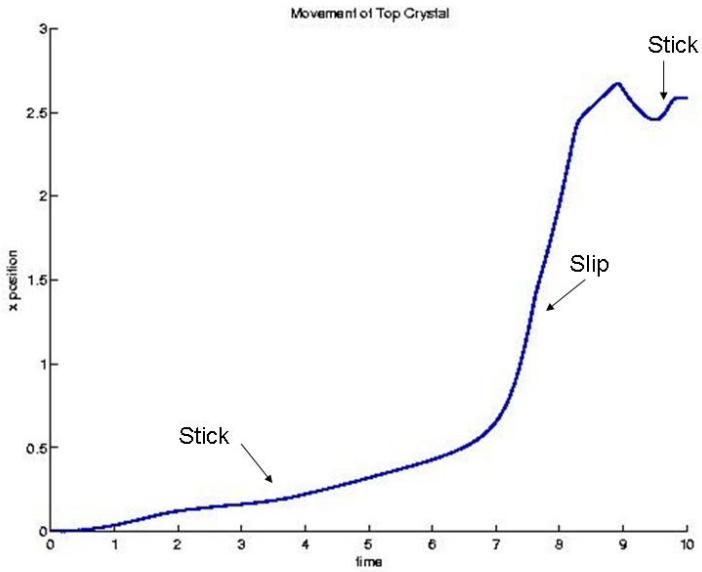

Figure 7: Movement of the top crystal

The crystal is sticking when the x-position of the crystal moves very slowly. Slip begins happening around $\tilde{t} = 7$ when the x-position of the crystal changes very rapidly. The top crystal sticks starts to stick again around $\tilde{t} = 9$.

Another way to view the stick-slip motion is by looking at the force exerted by the spring as a function of time. Figure 8 shows a steady increase in force until some critical force is achieved.

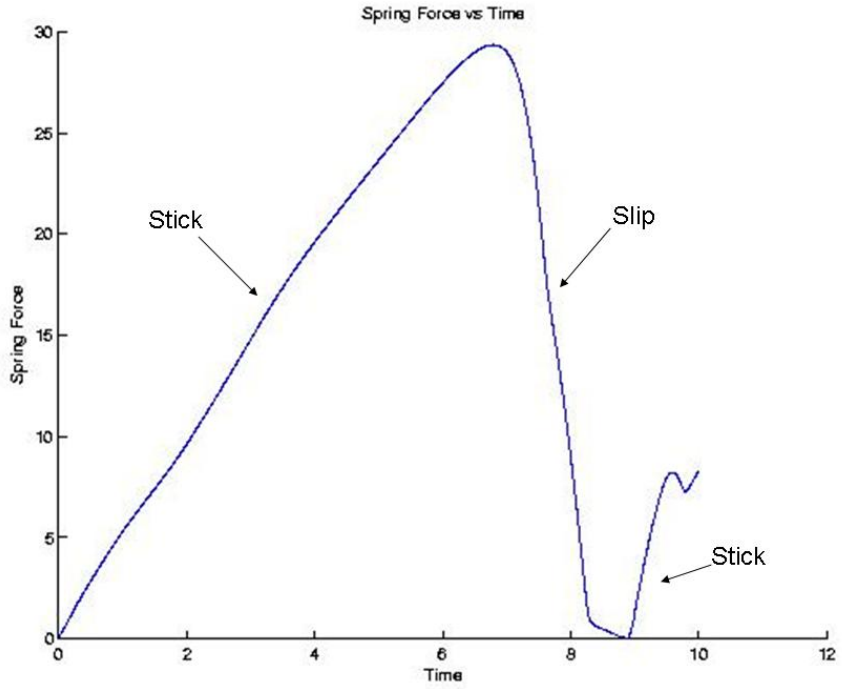

Figure 8: Spring force vs time

The top crystal sticks until the critical force is exceeded. The crystal then slips allowing the spring to compress. As the spring quickly compresses, the force exerted by the spring drastically decreases. Once the spring is compressed, the crystal starts to stick again and the force of the spring begins to increase again.

Chapter 4: Proper Orthogonal Decomposition

Proper Orthogonal Decomposition (POD) also referred to as Karhunen-Loève Decomposition, Principal Component Analysis, or Hotelling Transform, is often combined with a Galerkin projection to generate reduced-order models for large, complex systems (Lall, Marsden, and Glavaški; Prajna; Rowley). This powerful technique has been applied to a number of different areas of analysis including turbulent flows, image processing, data compression, human speech, and human faces. (Rowley; Ly and Tran; Ravindran; Rowley, Colonius, and Murray) The goal with POD is to determine the optimal subspace capable of capturing the dynamics of a high dimensional system. The dynamics of the high-dimensional system is then projected onto the subspace by using a Galerkin projection, thus producing a reduced-order model. The discussion of POD presented here is based on details provided in [Lall, Marsden, and Glavaški; Prajna; Rowley].

For a nonlinear, autonomous system described by

$$\dot{w} = f(w(t)) \text{ for } w \in \Re^n \qquad (32)$$

the goal is to find a reduced-order model

$$\dot{a} = g(a(t)) \text{ for } a \in \Re^m, \text{ m} << \text{n}. \qquad (33)$$

The POD technique determines a subspace, S, based on data from experiments or computer simulations. From the data, a set of data points or "snapshots", $\{w_1, w_2, \ldots, w_n\}$ are extracted. Given a set of data points, the POD approach aims to find a projection operator P that minimizes the square of the errors where the error is

calculated as the perpendicular distance from the original data point and the projected point in S as calculated by

$$\sum_{m=1}^{n} \left\| w^m - Pw^m \right\|. \qquad (34)$$

To determine the projection operator, P, the data points are then used to construct a correlation matrix

$$R = \sum_{i=1}^{n} (w_i)(w_i)^* \qquad (35)$$

with $\lambda_1 \geq \lambda_2 \geq \ldots \lambda_n$ the ordered eigenvalues of R and $\varphi_1, \varphi_2, \ldots \varphi_n$ the orthonormal eigenvectors of R. Here, the symbol * represents the transpose function. Then the minimum of (34) "over all projections of rank m is given by

$$\sum_{k=m+1}^{n} \lambda_k$$

and in the original coordinates the projection matrix that achieves this is given by P = Q*Q where

$$Q = \begin{bmatrix} \phi_1 * \\ \phi_2 * \\ \vdots \\ \phi_{m*} \end{bmatrix} \qquad (36)$$

" (Prajna, 2). The eigenvectors $\phi_1, \phi_2, \ldots, \phi_m$ are referred to as the POD modes.

In order to determine the appropriate number of modes to use in the reduced-order system, the percent of total energy captured in the first m modes is calculated by

$$\% \text{ of total energy } = \frac{\sum_{i=1}^{m} \lambda_i}{\sum_{i=1}^{n} \lambda i} \times 100 \qquad (37)$$

The goal is to find a small value for m such that the percent of total energy is close to 100% (Lall, Marsden, and Glavaški, 3). The subspace constructed using the corresponding m eigenvectors is optimal in approximating the data set in that it maxizes the energy captured over all m-dimensional subspaces (Ravindran, 5).

Once the modes are calculated and the number of modes to be used is determined, the dynamics of the original system is projected onto the subspace using the Galerkin Projection method. If the reduced-order system described in equation (32) is of the form

$$\dot{a} = g(a(t)) \text{ for } a \in \Re^m, \qquad (38)$$

then

$$w(t) = Q * a(t) + r(t) \qquad (39)$$

where Q is the matrix calculated earlier in equation 36. Following this,

$$Q * \dot{a}(t) + \dot{r}(t) = f(Q * a(t) + r(t)). \qquad (40)$$

The residual, $\dot{r}(t)$ is forced to be orthogonal to the subspace so that $\Pr(t) = 0$ (Lall, Marsden, and Glavaški, 3). Thus

$$Q * \dot{a}(t) = f(Q * a(t) + r(t)). \qquad (41)$$

Pre-multiplying both sides by Q results in

$$\dot{a}(t) = Qf(Q * a(t) + r(t)) \qquad (42)$$

"This describes the exact dynamics of the system on S. The final step in the model reduction is to assume that the projection has been chosen in such a way that r(t) is small" (Prajna, 2). The end result is a reduced-order system with

$$\dot{a}(t) = Qf(\dot{Q} * a(t)) \qquad (43)$$

Chapter 5: Basic POD Applied to Model

Using this simulation from Chapter 3, data points were collected every $\tilde{t} = 0.005$, producing 2000 data points or "snapshots". These snapshots consisted of the position and velocity of each lubricant atoms ($\tilde{x}, \tilde{y}, \tilde{x}', \tilde{y}'$) as well as the position and velocity of the top crystal ($\Delta\tilde{\alpha}, \Delta\beta, \Delta\tilde{\alpha}', \Delta\tilde{\beta}'$).

The POD approach begins by constructing the correlation matrix, R, of these snapshots. The ordered eigenvalues are then used to determine the POD modes. Figure 9 shows a plot of the eigenvalues of R versus their index in the ordered sequence. Given how the largest eigenvalue is much larger than the rest, the magnitude of the eigenvalues compared to each other can better be seen in Figure 10 which shows a plot of the log of the eigenvalues of R versus their index in the ordered sequence.

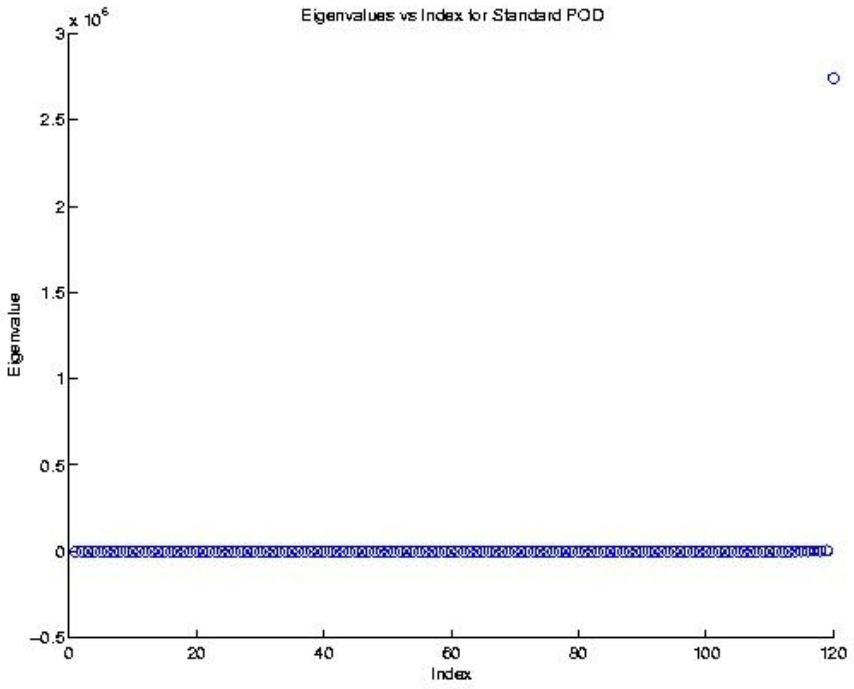

Figure 9: Eigenvalues versus index for correlation matrix of standard POD

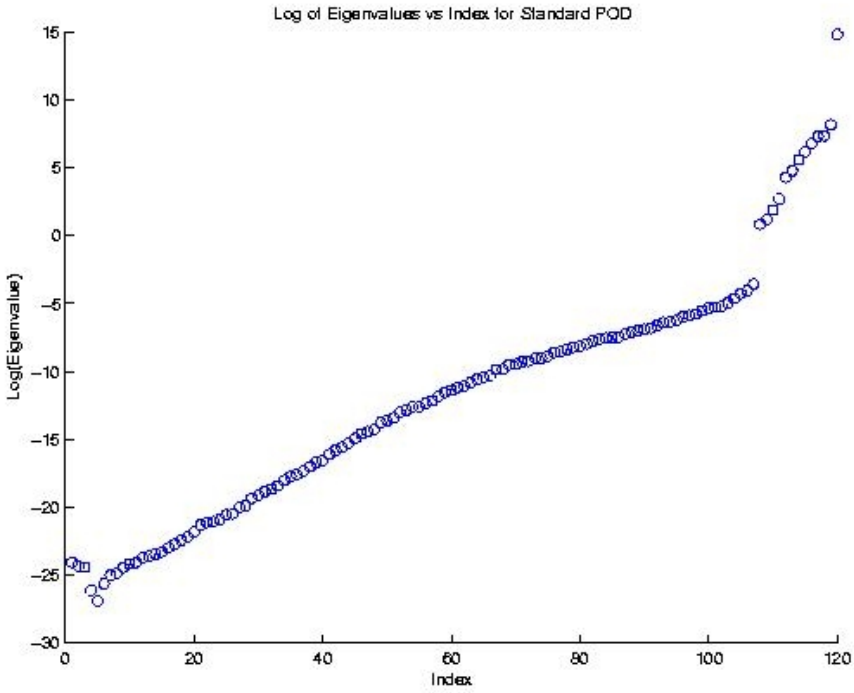

Figure 10: Log of Eigenvalues vs index for correlation matrix of standard POD

The difficulty with using POD to produce a reduced-order model is knowing how many modes are needed for a reduced order model. Looking at the plots in Figures 9 and 10 can help in determining an appropriate number of modes to use for constructing a subspace. For the largest 13 eigenvalues, the percent of total energy is over 99.99%, which is a good sign that the model reduction will be able to closely capture the dynamics of the original model. Using the eigenvectors associated with the largest 13 eigenvalues as the POD modes, a projection matrix is constructed and a Galerkin method is applied to produce a reduced-order model of the full-scale system. The simulation of this low-dimensional system is done in Matlab using the same "ode15s" function and parameters as were used with the full-scale model. The resulting trajectories can be seen in Figure 11(b).

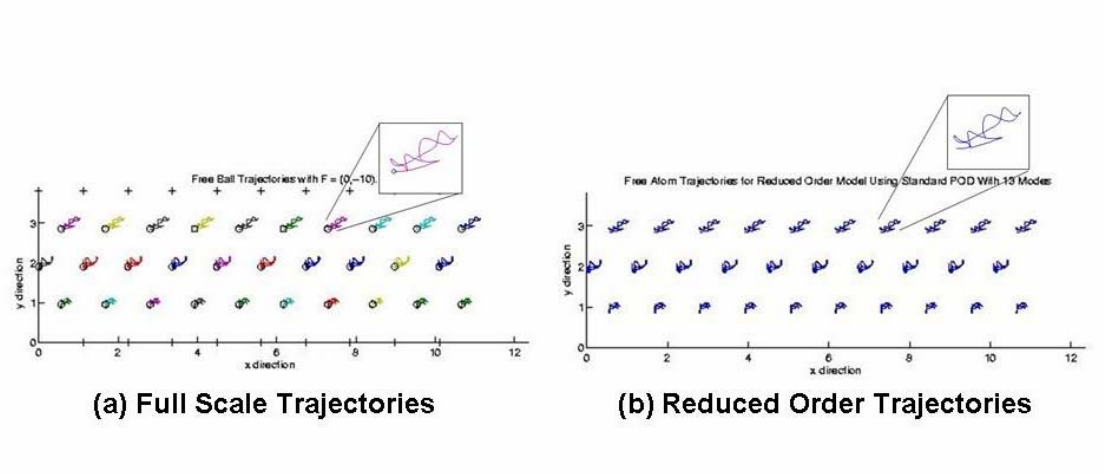

Figure 11: Lubricant atom trajectories for reduced order model using standard POD with 13 modes

In addition, Figure 12 shows the movement of the top crystal for the reduced-order model.

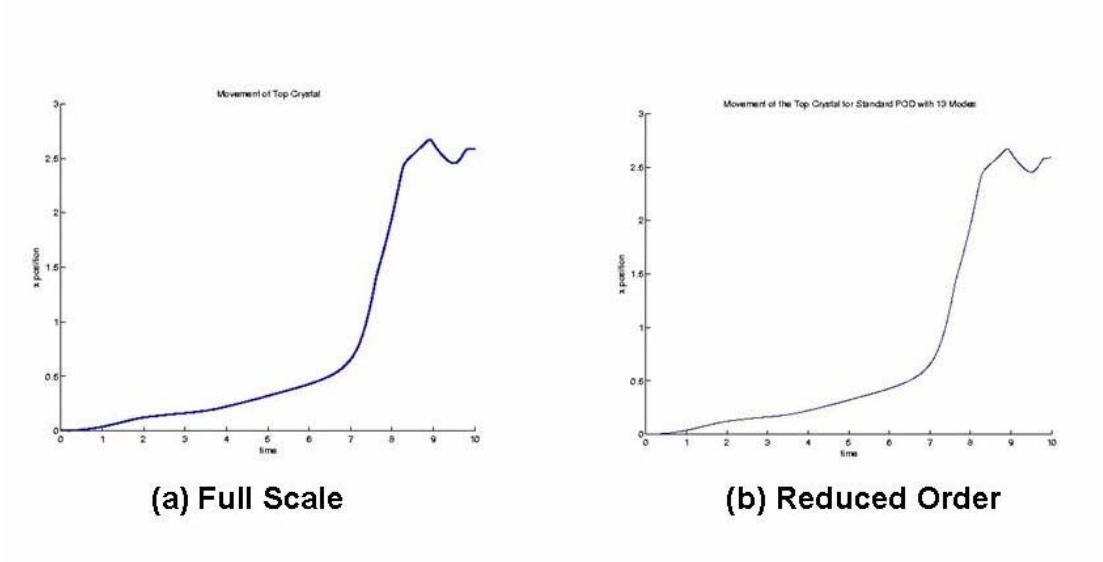

Figure 12: Movement of top crystal for reduced order model using standard POD with 13 modes

An RMS (Root Mean Square) error is calculated for the difference between the trajectories of the original system and the trajectories of the reduced-order system. In addition, an RMS error is calculated for the difference between the movement of the top crystal in the original system and the movement of the top crystal in the reduced-order system. The RMS errors for the reduced-order model using 13 modes are 6.3593e-4 for the error in the lubricant atoms and 3.4666e-4 for the error in the top crystal. The number of modes used in the reduced-order model was varied slightly with the results presented in Table 1.

Number of Modes	% Total Energy	RMS Error for Lubricant Atoms	RMS Error for Top Crystal Position
8	99.9011	0.1459	0.4380
9	99.9888	0.1261	0.2903
11	99.9998	0.0431	0.0237
13	99.9999	6.3593e-4	3.4666e-4
15	99.9999	5.8051e-4	4.0854e-4

Table 1: Results for reduced-order model with varying number of modes

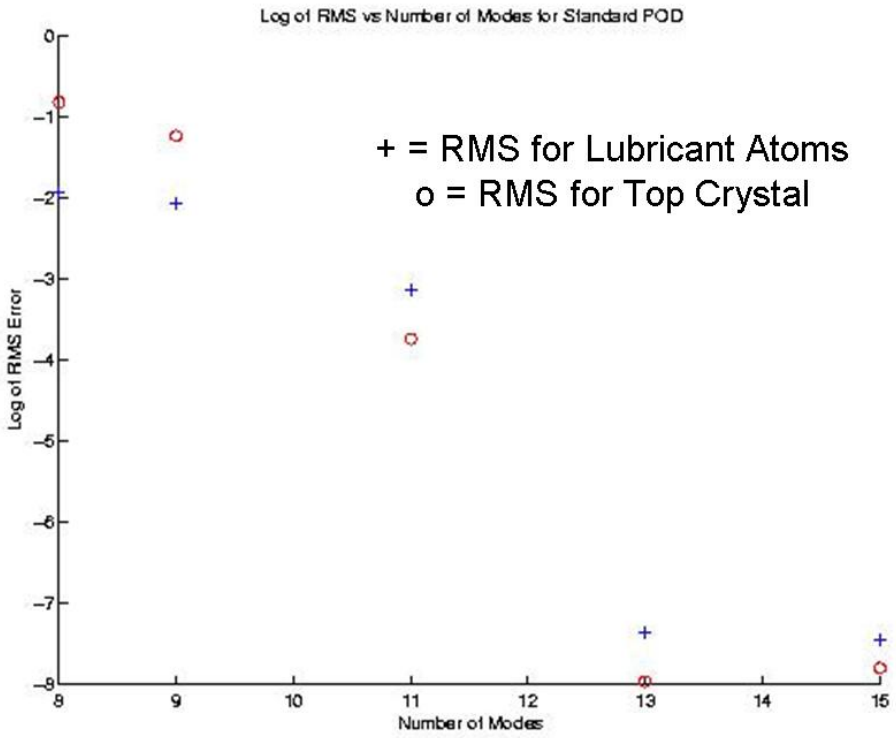

Figure 13: RMS Error vs Number of Modes for Standard POD Approach

As can be seen by these results, the straightforward application of the POD technique applied to the nanoscale slip-stick friction problem is able to yield a reduced-order model that closely captures the dynamics of the original model. In this case, 13 modes are able to create a reduce-order system that accurately models the original system

Chapter 6: Modified POD Approach Applied to Model

While for this simple simulation, the standard POD approach clearly was able to produce an accurate reduced-order model, the standard POD approach is known to have its limitations. "Though POD modes are very effective (indeed optimal) at approximating a given dataset, they are not necessarily the best modes for describing the dynamics that generate a particular dataset, since low-energy features may be critically important to the dynamics" (Rowley, 5). For the nanoscale friction problem the dynamics of interest, the time when the top crystal is slipping, occurs very quickly and is thus underrepresented in the snapshot collection. In particular, of the 2000 snapshots used for constructing a reduced-order model, 1459 were for stick and 541 were for slip – only 27% of the snapshots captured the slip dynamics.

In hopes of finding a better reduced-order model, the standard POD approach was modified to make sure that the slip dynamics get significant weight in the subspace construction. This modified approach consists of determining a set of "stick" modes and a set of "slip" modes that are used in combination for determining the reduced-order model. In particular, since the free-atom configuration is stable during "stick" and unstable during "slip", each data point that was collected was evaluated to determine its stability. The stability of each snapshot was determined using the Hessian matrix for the potential energy described in Chapter 3. Then the standard POD technique was applied separately to the set of stable data points and to the set of unstable data points. The results of the stable modes and unstable modes were combined for the Galerkin projection.

We use the same simulation that we used with the standard POD approach. Snapshots are collected that consisted of the position and velocity of each lubricant atoms ($\tilde{x}, \tilde{y}, \tilde{x}', \tilde{y}'$) as well as the position and velocity of the top crystal ($\Delta\tilde{\alpha}, \Delta\beta, \Delta\tilde{\alpha}', \Delta\tilde{\beta}'$). For each snapshot, the Hessian matrix for the potential energy is calculated as in Chapter 3 and the eigenvalues are evaluated to determine the stability of the data point. A subset of the snapshots is constructed that consists of the stable data points and another subset is constructed that consists of the unstable data points.

These two subsets of snapshots are then used with the standard POD technique to produce two sets of POD modes. A correlation matrix, $R_{stable,}$ is constructed for the stable data points and a separate correlation matrix, $R_{unstable}$, is constructed for the unstable data points. The ordered eigenvalues of each correlation matrix are then used independently to determine the POD modes. Figure 14 shows a plot of the eigenvalues of R_{stable} versus their index in the ordered sequence. Given how the largest eigenvalue is much larger than the rest, the magnitude of the eigenvalues compared to each other can better be seen in Figure 15 which shows a plot of the log of the eigenvalues of R_{stable} versus their index in the ordered sequence.

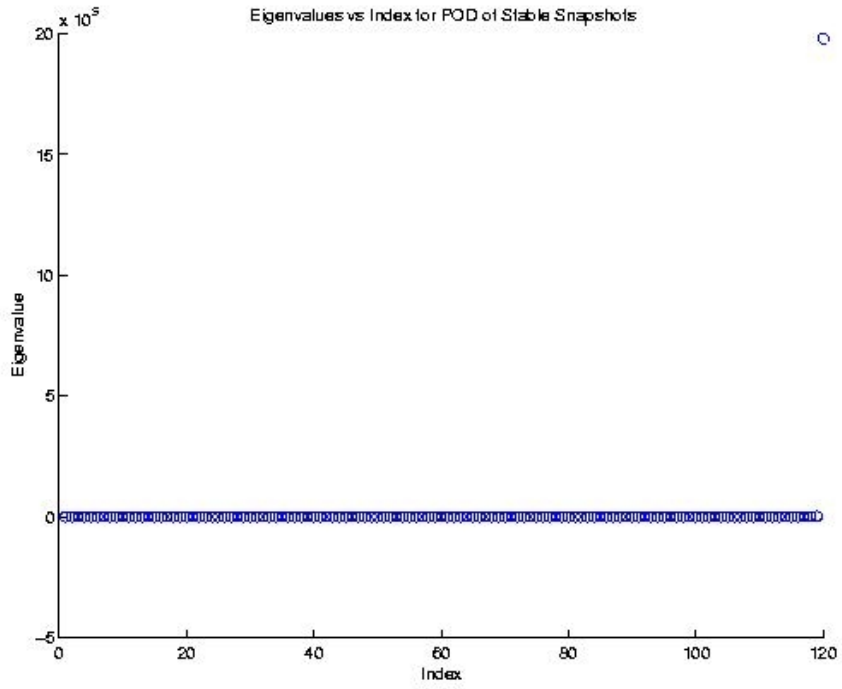

Figure 14: Eigenvalues versus Index for the Correlations Matrix of Stable Snapshots

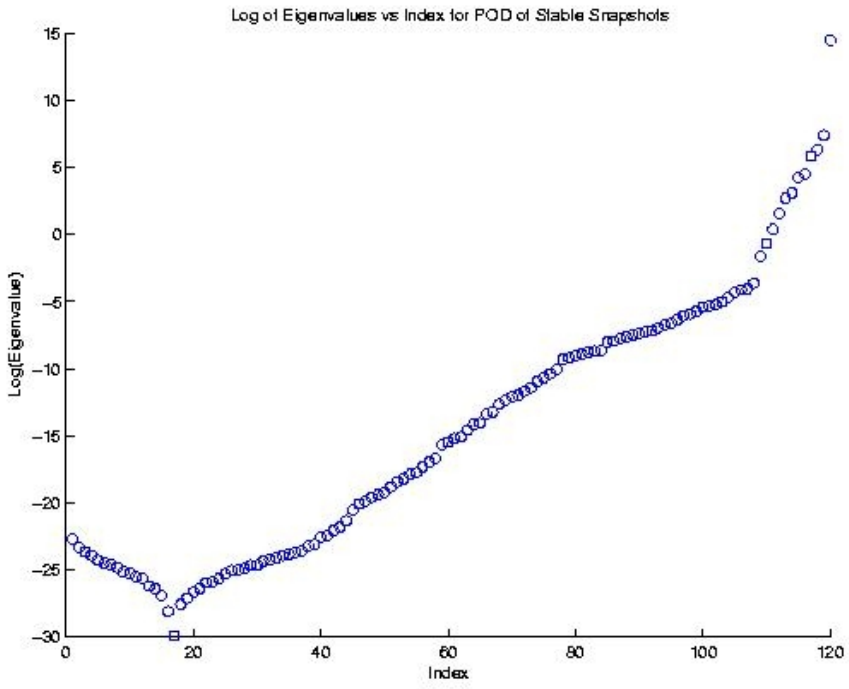

Figure 15: Top Eigenvalues, Except Largest versus Index for Correlation Matrix of Stable Snapshots

Likewise, Figure 16 shows a plot of the eigenvalues of $R_{unstable}$ versus their index in the ordered sequence. Given how again the largest eigenvalue is much larger than the rest, the magnitude of the eigenvalues compared to each other can better be seen in Figure 17 which shows a plot of the log of the eigenvalues of $R_{unstable}$ versus their index in the ordered sequence.

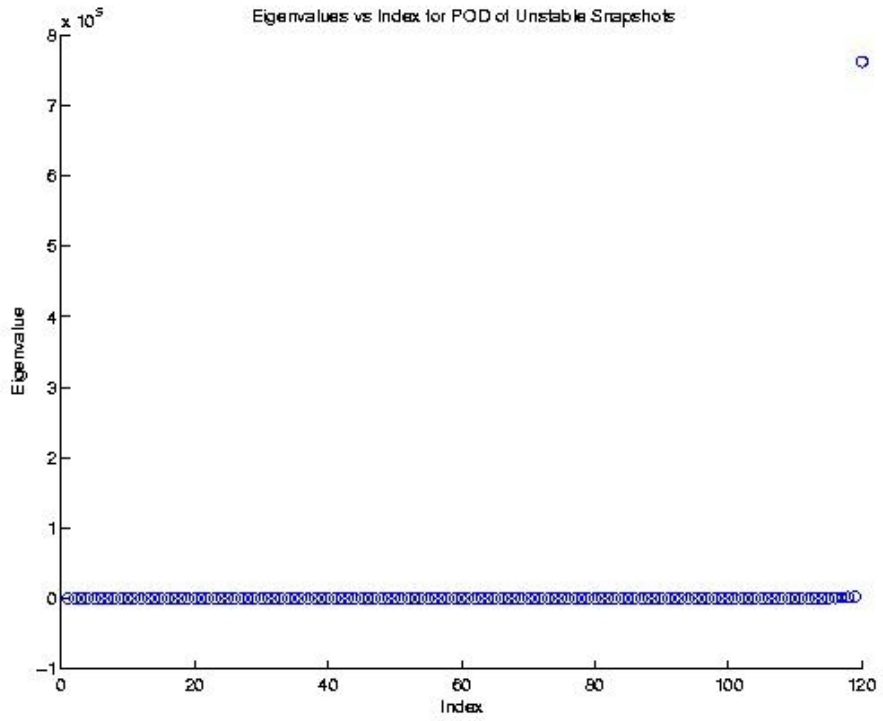

Figure 16: Eigenvalues versus Index for Correlation Matrix of Unstable Snapshots

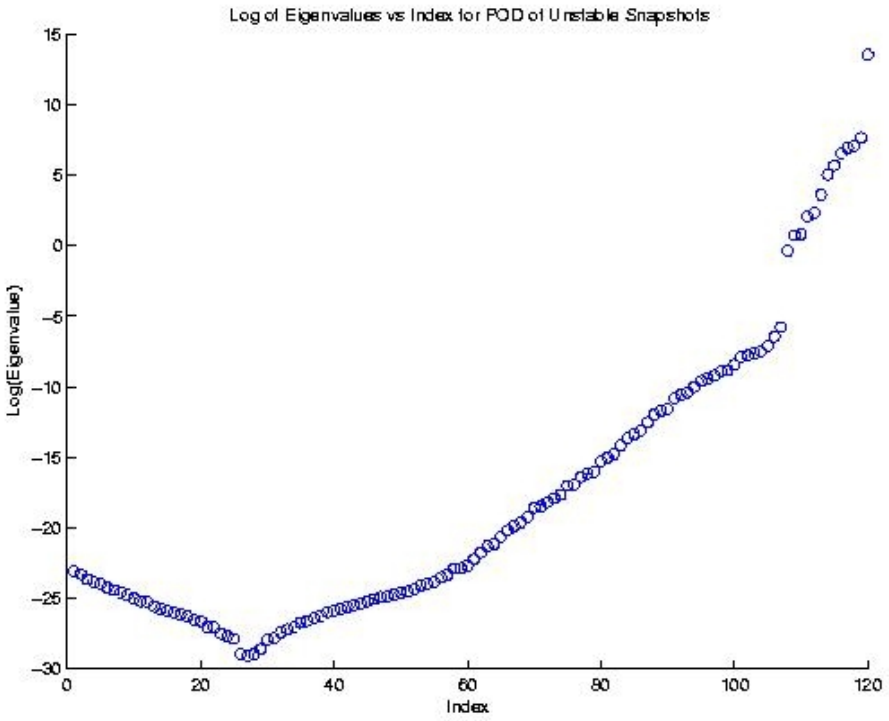

Figure 17: Top Eigenvalues, except Largest versus Index for Correlation Matrix of Unstable Snapshots

The difficult in choosing the number of modes to use for the reduced-order model becomes even more difficult with this modified approach. Now, we need to determine both the number of stable modes and the number of unstable modes to use. The plots in Figures 14 through 17 are examined to try and determine an appropriate number of stable modes and an appropriate number of unstable modes to use for constructing a subspace.

With the largest 8 eigenvalues from the stable correlation matrix, the percent of total "stick" energy represented is 99.9971% and with the largest 5 eigenvalues from the unstable correlation matrix, the percent of total "slip" energy represented is 99.9343%. As was states in chapter 4, for POD we aim to find the smallest number of modes where the percent of total energy is close to 100% (Lall, Marsden, and

Glavaški, 3). Thus, using 8 stable modes and 5 unstable modes we should expect to be able to accurately approximate the original model.

The POD modes for the reduced-order model are the combination of the stable modes based on the eigenvectors associated with the largest 8 eigenvalues from the stable correlation matrix and the unstable modes based on the eigenvectors associated with the largest 8 eigenvalues from the unstable correlation matrix. A projection matrix is constructed from these modes and a Galerkin method is applied to produce a reduced-order model of the full-scale system. The resulting trajectories for the reduced-ordered model constructed from the modified POD approach can be seen in Figure 18.

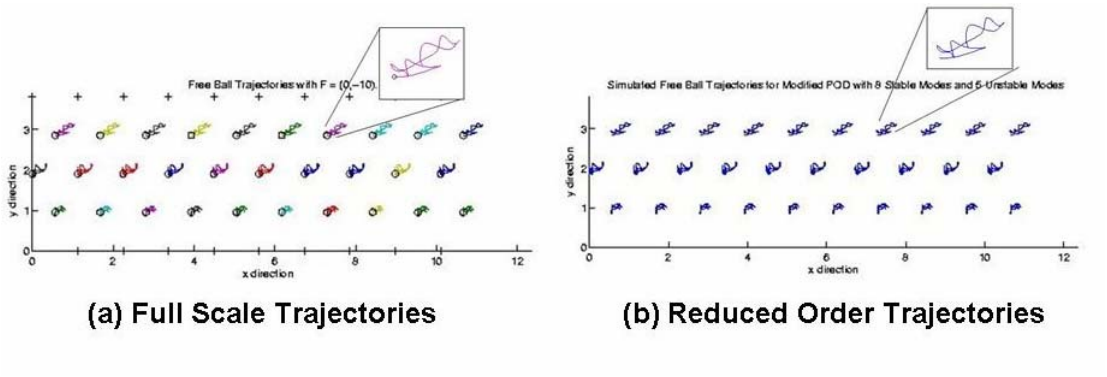

Figure 18: Lubricant Atom Trajectories for Reduced Order Model Using 8 Stable Modes and 5 Unstable Modes for Modified POD

In addition, Figure 19 shows the movement of the top crystal for the reduced-order model.

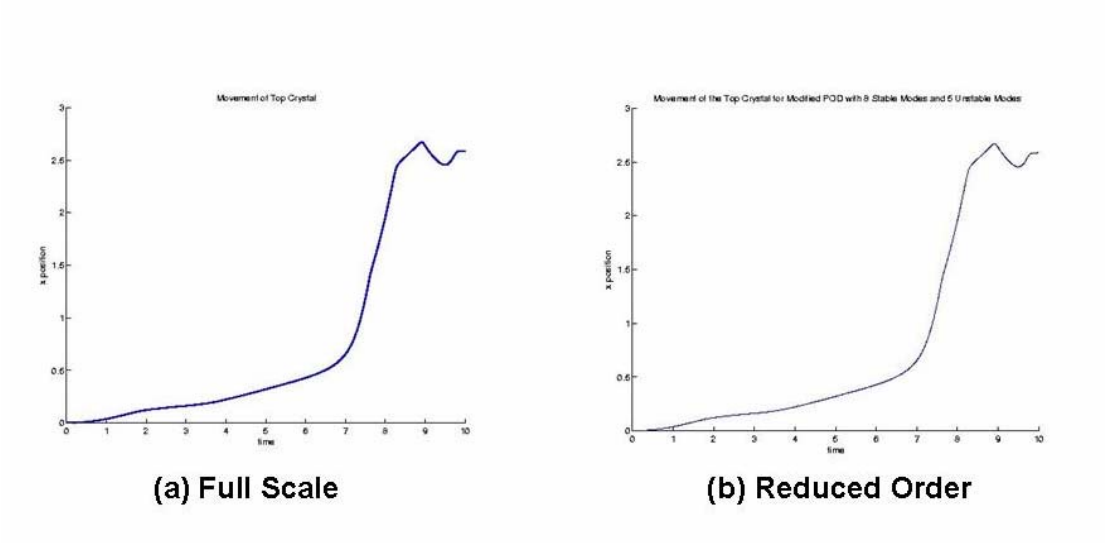

Figure 19: Movement of the Top Crystal for Reduce Order Model Using 8 Stable Modes and 5 Unstable Modes for Modified POD

Again, the RMS error is calculated for the difference between the trajectories of the original system and the trajectories of the lubricant atoms of the reduced-order system and for the difference between the movement of the top crystal in the original system and the movement of the top crystal in the reduced-order system. The RMS error for the reduced-order model using 8 stable modes and 5 unstable modes is 4.5898e-4 for the lubricant atoms and 2.1859e-4 for the top crystal. The number of modes used in the reduced-order model was varied slightly with the results presented in Table 2.

Number of Stable Modes	Number of Unstable Modes	% of Total "Stick" Energy	% of Total "Slip" Energy	RMS Error of Lubricant Atoms	RMS Error of Top Crystal Position
5	3	99.9300	99.8823	0.1201	0.2449
5	8	99.9300	99.9989	0.0045	0.0053
6	3	99.9884	99.8823	0.0652	0.0530
6	5	99.9884	99.9343	0.0430	0.0231
6	7	99.9884	99.9703	0.0016	0.0011
8	5	99.9971	99.9343	4.5898e-4	2.1859e-4
8	7	99.9971	99.9703	3.7901e-4	1.2795e-4

Table 2: Results for Reduced-Order Model Using Modified POD Technique

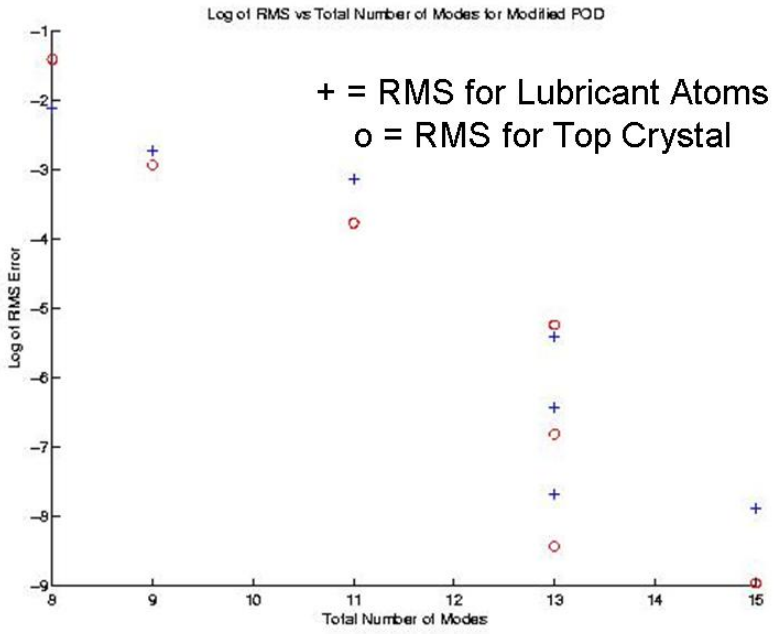

Figure 20: RMS vs Total Number of Modes for Modified POD

As can be seen by these results, the modified version of the POD technique applied to the nanoscale slip-stick friction problem is also able to yield a reduced-order model that closely captures the dynamics of the original model. For a given number of modes, using the modified POD approach, there exists a combination of stable and unstable modes that is able to more accurately describe the system than the reduced-order system constructed using a standard POD approach with the same number of modes. It should be noted, that while there exists a combination of stable and unstable modes that produces better results than the standard approach, there also exists one or more combinations of stable and unstable modes that actually produce worse results.

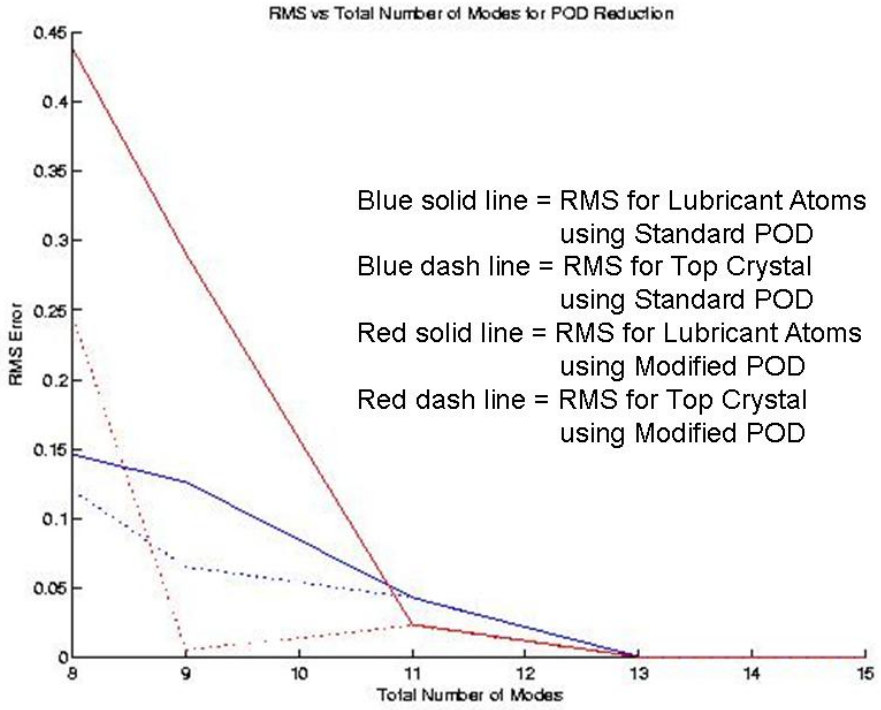

Figure 21: RMS Error vs Total Number of Modes for POD

Chapter 7: Conclusions and Suggestions for Future Research

In comparing the results from the standard POD approach and the modified POD approach, it is clear that the modified POD approach is able to more accurately approximates the full-scale system than the standard POD approach for the same number of modes. For example, in this case, the standard POD method produced good results with 13 modes while the modified POD technique produced better results with 13 modes (8 stable and 5 unstable). The original model consisted of 4 variables (x,y,x., y.) for each atom. For this experiment, there were 30 free lubricant atoms and 20 crystal atoms, 10 of which were stationary. Thus, 160 variables would describe the position and velocity of each atom in the model. Representing the top crystal atom as a single unit reduced the system to 124 variables. Using either the standard POD or modified POD approach with 13 modes, the original model can be accurately reduced to a system of 17 variables. Thus, either method of model reduction reduced the dimensions of the model by almost 90% while closely capturing the dynamics of the full-scale model.

While the modified POD approach shows promise at producing a more accurate, lower-dimensional system, there is a computation trade-off of this method. The modified technique requires the calculation of eigenvalues for two large matrices (each 120x120 in this experiment). So, the modified POD requires more computations for the model reduction than the standard POD but the modified POD can more effectively capture the dynamics of the original system with the same number of modes as the standard POD approach. In addition, additional computation is needed to determine the appropriate combination of stable and unstable modes for

the modified POD approach. Further research should be done to explore how to determine the best combination of stable and unstable modes for the modified approach and how the number of modes needed for an accurate model reduction with both the standard POD and the modified POD grows with the size of the system.

The experiment presented in the paper is a simple experiment. There are a number of variations of this experiment that can be used to evaluate how the modified POD method compares with the standard POD such as the lubricant made up of molecules rather than single atoms and imperfect crystal surfaces. In addition to determining how well the standard and modified POD methods hold up under varying experiments, these methods should also be compared against other model reduction techniques such as Balanced Truncation. In particular, the methods presented here should be compared against the Proper Orthogonal Decomposition using neural networks approach that was used by Y. C. Liang, W. Z. Lin, H. P. Lee, S. P. Lim, K. H. Lee, and H. Sun for a different type of experiment (515-532). Lastly, the model reductions constructed for this experiment were based off of data from computer simulations. Both the standard and modified POD approaches should be evaluated using real data.

Appendix

Nomenclature – Presented in order of appearance in paper.

C	Compression force
v	Velocity
M_1	Number of atoms in the top crystal
M_2	Number of atoms in the bottom crystal
M	Total number of crystal atoms
N	Number of lubricant atoms
x_i	X-position of the i^{th} lubricant atom
y_i	Y-position of the i^{th} lubricant atom
α_i	X-position of the i^{th} crystal atom
β_i	Y-position of the i^{th} crystal atom
$\Delta\alpha$	Change in the X-position of the top crystal
$\Delta\beta$	Change in the Y-position of the top crystal
α_{i0}	Starting X-position of the i^{th} crystal atom
β_{i0}	Starting Y-position for the i^{th} crystal atom
m_{iLA}	Mass of the i^{th} lubricant atom
m_{iCA}	Mass of the i^{th} crystal atom
KE	Kinetic energy of the system
u()	Lennard Jones Potential
r	Distance between two atoms

r*	Equilibrium distance for the Lennard Jones Potential
ε,σ	Lennard Jones Potential parameters
PE_A	Potential energy due to atomic interaction
F	Spring force
K	Spring constant
Δ	Displacement of top crystal from equilibrium position
PE_B	Potential energy due to external forces on top crystal
t	Time
PE	Total potential energy of the system
m_{CA}	Mass of crystal atoms
m_{LA}	Mass of lubricant atoms
m_A	Mass of atoms
$\tilde{x}_i$	Nondimensionalized X-position of the i^{th} lubricant atom
L0	Nondimensionalized reference length
$\tilde{y}_i$	Nondimensionalized Y-position of the i^{th} lubricant atom
$\tilde{\alpha}_i$	Nondimensionalized X-position of the i^{th} crystal atom
$\tilde{\beta}_i$	Nondimensionalized Y-position of the i^{th} crystal atom
$\tilde{\Delta}\alpha$	Nondimensionalized change in X-position of the top crystal
$\tilde{\Delta}\beta$	Nondimensionalized change in Y-position of the top crystal
$\tilde{t}$	Nondimensionalized time
τ	Nondimensionalized temporal unit

$\widetilde{K}$	Nondimensionalized spring constant
$\widetilde{C}$	Nondimensionalized compression force
$\widetilde{v}$	Nondimensionalized velocity
d	Damping coefficient
H	Hessian matrix of the potential energy function
R	Correlation matrix for standard POD
P	Projection matrix for standard POD
S	POD subspace
wi	The ith POD snapshot
Λi	The i^{th} ordered eigenvalue of the correlation matrix R
n	Order of full-scale system
m	Order of the reduced system
Φi	The i^{th} orthonormal eigenvector of the correlation matrix R
P*	Transpose of the projection matrix P
a	Variable for reduced order system
Rstable	Correlation matrix of the stable data points
Runstable	Correlation matrix of the unstable data points

Bibliography

Aranson, L. S., Tsimring, L. S., and Vinokur, V. M., "Stick-slip Friction and Nucleation Dynamics of Ultrathin Liquid Film", Physical Review B 65,125402, (2002): 1-7.

Brakke, Kenneth A., "The Surface Evolver and the Stability of Liquid Surfaces", Philosophical Transactions of the Royal Society London A, 1995, 1-8.

Gao, Jianping, Luedtke, W. D., Gourdon, D., Ruths, M., Israelachvili, N., and Landman, Uzi, "Frictional Forces and Atontons' Laws: From the Molecular to the Macroscopic Scale", J. Phys. Chem., B 108, (2004), 3410-3425.

Harrison, J. A., White, C. T., Colton, R. J., and Brenner, D. W., "Molecular-dynamics Simulations of Atomic-Scale Friction of Diamond Surfaces", Physical Review B 46 (1992): 9700-9708.

He, Gang, and Robbins, Mark O., "Simulation of the Kinetic Friction Due to Absorbed Surface Layers", Tribology Letters 0, (2006), 1-8.

Krim, Jacqueline, "friction at the Nano-Scale", Physics World, February 2005, http://physicsweb.org/articles/world/18/2/9

Lall, Sanjay, Marsden, Jerrold E., and Glavaški, Sonja, "Empirical Model Reduction of Controlled Nonlinear Systems", Technical Report CIT-CDS-98-008, (1998): 1-9.

Liang, Y. C, Lin, W. Z., Lee, H. P., Lim, S. P., Lee, K. H., and Sun, H., "Proper Orthogonal Decomposition and Its Applications – Part II: Model Reduction for MEMS Dynamical Analysis", Journal of Sound and Vibration 256 (2002): 515-532

Ly, Hung V. and Tran, Hien T., "Modeling and Control of Physical Processes using Proper Orthogonal Decomposition", to appear in Journal of Mathematical and Computer Modeling, (1999): 1-16.

Prajna, Stephen, "POD Model Reduction with Stability Guarantee", Proceedings of the IEEE Conference on Decision and Control (CDC), Maui, HI. (2003): 1-5.

Ravindran, S. S., "Proper Orthogonal Decomposition in Optimal Control of Fluids", http://library-dspace.larc.nasa.gov/dspace/jsp/bitstream/2002/14311/1/NASA-99-tm209113.pdf

Robbins, Mark O. and Müser, Martin H., "Computer Simulations of Friction, Lubrication and Wear," to appear in Modern Tribology Handbook, Edited by B.

Bhushan (CRC Press, Boca Raton, 2001), http://www.pha.jhu.edu/~mr/papers.html, 1-42.

Rowley, C.W., "Model Reduction for Fluids, Using Balanced Proper Orthogonal Decomposition" to appear in Int. J. on Bifurcation and Chaos, (2005), http://www.princeton.edu/~cwrowley/papers/bt_ijbc3.pdf, 1-21.

Rowley, Clarence W., Colonius, Tim, and Murray, Richard M., "Model Reduction for Compressible Flows using POD and Galerkin Projection", to appear Physica D (2003), http://green.caltech.edu/colonius/pdfs/RowleyColoniusMurray2004.pdf

Rozman, M. G, Urbakh, M., and Klafter, J., "Slip-Stick Motion and Force Fluctuations in a Drive Two-Wave Potential", Physical Review Letters 77 (1996): 683-686.

Schall, David, Padgett, Clifford W., and Brenner, Donald W., "Ad hoc Continuum-Atomistic Thermostat for Modeling Heat Flow in Molecular Dynamic Simulations", Molecular Simulation, Vol 31, No. 4, April 2005, 283-288.

Shapiro, Bruce E. and Hong Qian, "Hysteresis in Force Probe Microsopy: A Dynamical Systems Persepctive", Jornal of Theoretical Biology 194 (1998): 551-559.

Shimizu, Jun, Eda, Hiroshi, Yoritsune, Masashi, and Ohmura, Etsuji, "Molecular Dynamics Simulation of Friction on the Atomic Scale", Nanotechnology 9, (1998), 118-123.

Singer, I. L., "Friction and Energy Dissipation at the Atomic Scale: a Review", J. Vac. Sci. Technol. A 12(5), Sep/Oct 1994, 2605-2616.

Wells, D. A., Theory and Problems of Lagrangian Dynamics, Schaum's Outline Series, McGraw-Hill Book Company, New York, 1967.